Unpolarized emissivity with shadow and multiple reflections from random rough surfaces with the geometric optics approximation: application to Gaussian sea surfaces in the infrared band

Christophe Bourlier

The emissivity from a stationary random rough surface is derived by taking into account the multiple reflections and the shadowing effect. The model is applied to the ocean surface. The geometric optics approximation is assumed to be valid, which means that the rough surface is modeled as a collection of facets reflecting locally the light in the specular direction. In particular, the emissivity with zero, single, and double reflections are analytically calculated, and each contribution is studied numerically by considering a 1D sea surface observed in the near infrared band. The model is also compared with results computed from a Monte Carlo ray-tracing method.

OCIS codes: 290.5880, 000.5490, 010.4450, 260.3060, 280.0280.

1. Introduction

The emissivity of ocean surface in the atmospheric transmission windows is an important parameter for retrieving the sea surface temperature (SST) from radiometric sensors, located either on satellites or a platform close to the sea surface. It has been established that for an accuracy of 0.3 K on the SST, the error in the emissivity must be approximately 0.5%.[1] Consequently, the sea surface emissivity needs to be determined with accuracy.

Emissivity models developed in Refs. 1–4 neglected the dependence on the wind direction (isotropic surface), and the shadowing effect was ignored. The model presented in this paper is based on Refs. 5–7, in which a 2D rough sea surface with Gaussian and non-Gaussian statistics are considered, and in which the shadowing effect is taken into account. Nevertheless, unlike Ref. 5, Bourlier *et al.*[6,7] used no assumption on the derivation of the 2D illumination function. In addition, the effect of the wind direction on the emissivity is studied in detail.

As presented in Refs. 8–10, the emissivity can also be derived from the hemispherical reflectivity, for which the sea surface is assumed to be Gaussian, anisotropic, and the shadowing effect is ignored, unlike in Ref. 7. The hemispherical reflectivity is obtained from integrating the reflectivity over the half space above the sea surface. In this paper, this way is not used because the formulation is more complicated and the surface reflectivity is only necessary for the calculation of the sun glint. Indeed, as shown in Refs. 7–9, by using the radiative transfer method involving the atmospheric transmission coefficient, the surface reflectivity, and the surface emissivity, the thermal radiation received by the infrared sensor can be calculated. In this paper, I focus only on the intrinsic radiation of the sea surface related to its emissivity.

All quoted references ignored the multiple reflections. By considering a Gaussian rough sea surface, this effect has been investigated by Henderson, Theiler, and Villeneuve[11] from a Monte Carlo ray-tracing method. They showed for moderate wind speeds that the multiple reflection phenomenon occurs for emission angles larger than 40° and smaller than 80°. In this range, the difference between the emissivity with multiple reflections and single reflection can reach +0.03. Such a method requires a long computing

The author (christophe.bourlier@polytech.univ-nantes.fr) is with Institut de Recherche en Electrotechnique et Electronique de Nantes Atlantique, Radar team, Ecole polytechnique de l'université de Nantes, rue Christian Pauc, La Chantrerie, Boîte Postale 50609, 44306 Nantes, Cedex 9, France.

Received 8 August 2005; revised 14 November 2005; accepted 22 November 2005; posted 6 February 2006 (Doc. ID 63956).

0003-6935/06/246241-14$15.00/0

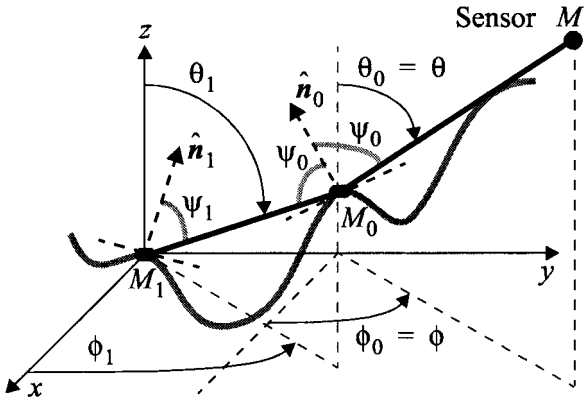

Fig. 1. Geometry used to calculate the zero- and the first-order emissivities. In the calculation of the emissivity, one sets $\theta_0 = \theta$ and $\phi_0 = \phi$.

time, because one needs to consider a great number of rays and surface realizations to reproduce the surface statistics and to average the emissivity. For any surface statistics and from an analytical approach, the purpose of this paper is to extend the previous works of Bourlier[6] by taking the multiple reflections into account in the calculation of the emissivity. Moreover, by considering a 1D sea surface, the contributions of the first (single reflection) and the second (double reflection) orders are analyzed against the emissivity calculated from zero reflection.

Before proceeding, let us note that this study of the rough sea surface emissivity is governed by several assumptions and approximations. In particular, the sea surface is assumed to be opaque for the infrared wavelengths of interest. The sea surface is modeled as being single valued and composed of a continuous collection of smooth facets with continuous first derivatives between adjacent facets. Each facet is assumed to be large with respect to the radiation wavelength, and geometrical optics is assumed to be a valid approximation for describing the interaction of radiation with any given facet. Atmospheric effects such as transmission loss and refractive are completely ignored. The electromagnetic radiation is taken to be unpolarized.

The paper is organized as follows: In Section 2, the emissivity with multiple reflections is derived by introducing the illumination function, and in Section 3 the illumination function is explicitly derived from the works of Bourlier *et al.*[12–14] Considering a 1D Gaussian rough sea surface, numerical results of the emissivity, and comparisons with a Monte Carlo ray-tracing method are presented in Section 4 for infrared wavelengths (4 and 10 μm). In addition, in the case where the first reflection is taken into account, to obtain better agreement with the Monte Carlo method, an empirical approach is presented.

2. Emissivity

In this section, the emissivity, $\varepsilon(\theta, \varphi)$, with N reflections is derived for any 2D stationary random rough surface. Let $\theta \in [0; \pi/2]$ be the emission angle with respect to the nadir of the sensor (Fig. 1) and $\phi \in [0; 2\pi]$ the azimuthal direction of the sensor. $\theta = 0°$ gives the nadir, whereas $\theta = 90°$ gives the horizon (grazing angle). For instance, $\{\phi = 0, 90, 180\}$ degrees corresponds to the up-, cross-, and downwind directions for a sea surface, respectively. The emissivity is defined as

$$\varepsilon(\theta, \phi) = \sum_{n=0}^{n=N} \varepsilon_n(\theta, \phi).$$

In the above equation, if no reflection occurs, then $\varepsilon = \varepsilon_0$, corresponding to the zero-order emissivity derived in the Subsection 2.A. If a single reflection occurs, then $\varepsilon = \varepsilon_0 + \varepsilon_1$. In the Subsection 2.B, the first-order emissivity, ε_1, is derived. Subsection 2.C presents the n-order emissivity, $\varepsilon_n(\theta, \phi)$.

A. Zero-Order Emissivity

The calculation of the zero-order emissivity, $\epsilon_0(\theta, \phi)$, is presented in Ref. 6 in detail and is summarized in this subsection. One sets $\theta_0 = \theta$ and $\phi_0 = \phi$.

For a horizontal plane, the emissivity is given by $1 - |r(|\psi_0|)|^2$, where ψ_0 is the angle between the normal to the plane and the direction of observation. Since the electromagnetic radiation is taken to be unpolarized, the reflection coefficient is $|r|^2 = (|r_v|^2 + |r_H|^2)/2$. r_V is the Fresnel coefficient defined in the V polarization (the electric vector parallel to the incidence plane), and r_H is the Fresnel coefficient defined in the H polarization (the electric vector orthogonal to the incidence plane). They are expressed as follows:

$$r_V(\psi_0) = \frac{n \cos \psi_0 - \cos \psi_0'}{n \cos \psi_1 + \cos \psi_0'},$$

$$r_H(\psi_0) = \frac{\cos \psi_0 - n \cos \psi_0'}{\cos \psi_1 + n \cos \psi_0'}, \quad (1)$$

where n is the sea refraction index (the air refraction index is assumed to be equal to 1), and ψ_0' is the refraction angle obtained from the Snell–Descartes law, $\sin \psi_0' = \sin \psi_0 / n$.

The incident power intercepted by a surface element dS_0 of rough surface, which is modeled as a collection of facets, is unit intensity × the area element projected onto the incident wavefront, i.e., $\hat{\mathbf{n}}_0 \cdot \hat{\mathbf{m}}_0 = \cos \psi_0$ (Fig. 1) with $\hat{\mathbf{m}}_0 = \overrightarrow{M_0 M}$. $\hat{\mathbf{m}}_0 = (\cos \phi_0 \sin \theta_0, \sin \phi_0 \sin \theta_0, \cos \theta_0)$ is the unitary vector giving the direction of observation, and $\hat{\mathbf{n}}_0 = (-\gamma_{x,0}, -\gamma_{y,0}, 1)/(1 + \gamma_{x,0}^2 + \gamma_{y,0}^2)^{1/2}$ is the unitary vector normal to dS_0, in which $\{\gamma_{x,0}, \gamma_{y,0}\}$ are the surface slopes in the up ($\phi_0 = 0°$) and cross ($\phi_0 = 90°$) directions, respectively. Thus

$$\cos[\psi_0(\theta_0, \phi_0; \gamma_{x,0}, \gamma_{y,0})] = \hat{\mathbf{n}}_0 \cdot \hat{\mathbf{m}}_0 = \frac{\cos\theta_0 - (\gamma_{x,0}\cos\phi_0 + \gamma_{y,0}\sin\phi_0)\sin\theta_0}{\left(1 + \gamma_{x,0}^2 + \gamma_{y,0}^2\right)^{1/2}}. \quad (2)$$

Then, if the local emissivity of a facet is $1 - |r(|\psi_0|)|^2$, the local emissivity of the surface element $dS_0 = dxdy(1 + \gamma_{x,0}^2 + \gamma_{y,0}^2)^{1/2}$ in direction $\hat{\mathbf{m}}_0$ and defined according to the plane (x, y) is $(1 - |r(|\psi_0|)|^2)\cos\psi_0(1 + \gamma_{x,0}^2 + \gamma_{y,0}^2)^{1/2}$. In addition, this emissivity must be divided by $\cos\theta$ because the power emanating from the surface and measured by the receiver with respect to the emission angle θ is divided by $\cos\theta$. From Eq. (2), the zero-order local emissivity is then given by

$$\epsilon_{l0}(\theta, \phi; \gamma_{x,0}, \gamma_{y,0}) = [1 - |r(|\psi_0|)|^2]g_0, \quad (3)$$

where

$$g_0 = \frac{\cos\psi_0\left(1 + \gamma_{x,0}^2 + \gamma_{y,0}^2\right)^{1/2}}{\cos\theta_0} = 1 - (\gamma_{x,0}\cos\phi_0 + \gamma_{y,0}\sin\phi_0)\tan\theta_0. \quad (4)$$

The emissivity measured by a sensor is equal to the local emissivity averaged over the statistical variables that depend on the local emissivity. For the zero-order emissivity, these variables are the surface slopes $\{\gamma_{x,0}, \gamma_{y,0}\}$ defined at the point M_0. Thus, by taking the zero-order *statistical* illumination function, S_0, into account the zero-order *average* emissivity, $\epsilon_0(\theta, \phi)$, is given by

$$\varepsilon_0(\theta, \phi) = \langle[1 - |r(|\psi_0|)|^2] \times g_0 \times \bar{S}_0\rangle_0, \quad (5)$$

where the ensemble average operator $\langle\cdots\rangle_0$ is given by

$$\langle\cdots\rangle_0 = \int_{-\infty}^{+\infty}\int_{-\infty}^{+\infty}(\cdots)p_s(\gamma_{x,0},\gamma_{y,0})d\gamma_{x,0}d\gamma_{y,0}. \quad (6)$$

p_s stands for the slope probability density function (PDF), and S_0 is the probability that the sensor illuminates the point M_0. Since the local emissivity does not depend on the surface height, the statistical illumination function $S_0(\gamma_{x,0}, \gamma_{y,0}, z_0)$ can be averaged over the height z_0 corresponding to $\bar{S}_0(\gamma_{x,0}, \gamma_{y,0})$ in Eq. (5). It will be derived in Section 3.

B. First-Order Emissivity

Let M_1 be an arbitrary point on the surface (Fig. 1). The ray emanating from this point has an emission angle θ_1 and an azimuthal direction ϕ_1. Let us suppose that this ray intercepts the surface at the point M_0. This point is observed from a sensor with an emission angle $\theta = \theta_0$ and an azimuthal direction $\phi = \phi_0$. If the ray emanating from the point M_1 does not cross the surface, the emissivity is given by Eq. (5) in which $\{\theta, \phi, \psi_0\}$ become $\{\theta_1, \phi_1, \psi_1\}$. In this subsection, it is proposed to derive the emissivity when a single reflection occurs.

At the point M_1, the local emissivity of the facet, ϵ_{l1}, is expressed as $\epsilon_{l1} = 1 - |r(|\psi_1|)|^2$, where ψ_1 is the angle between the local normal to the facet, $\hat{\mathbf{n}}_1$, and the ray (M_1M_0) (Fig. 1). At the point M_0, the local emissivity, ϵ_{l0}, is then given by $\epsilon_{l0} = \epsilon_{l1} \times |r(|\psi_0|)|^2 \times g_0$, where ψ_0 is the angle between the local normal to the facet $\hat{\mathbf{n}}_0$ and the ray (M_0M), and g_0 is the projection function (in other words, related to the "effective area" of the local facet defined along the emission angle θ) expressed from Eq. (4). The emissivity measured by a sensor is equal to the local emissivity averaged over the statistical variables that depend on the local emissivity. These variables are the surface slopes $\{\gamma_{x,0}, \gamma_{y,0}\}$ and $\{\gamma_{x,1}, \gamma_{y,1}\}$ defined at the points M_0 and M_1, respectively. In addition, to be consistent with the geometric optics approximation, the statistical correlation between M_0 and M_1 is omitted. Thus by taking the first-order statistical illumination function, S_1, into account, the first-order average emissivity, $\epsilon_1(\theta, \phi)$, is given by

$$\epsilon_1(\theta, \phi) = \langle[1 - |r(|\psi_1|)|^2] \times |r(|\psi_0|)|^2 \times g_0 \times \bar{S}_1\rangle_1, \quad (7)$$

where the ensemble average operator $\langle\cdots\rangle_1$ is given by

$$\langle\cdots\rangle_1 = \int_{-\infty}^{+\infty}\int_{-\infty}^{+\infty}(\cdots)p_s(\boldsymbol{\gamma}_0)p_s(\boldsymbol{\gamma}_1)d\boldsymbol{\gamma}_0d\boldsymbol{\gamma}_1, \quad (8)$$

with $\boldsymbol{\gamma}_i = [\boldsymbol{\gamma}_{x,i} \quad \boldsymbol{\gamma}_{y,i}]$ and $i = \{0, 1\}$. S_1 gives the probability that the ray (M_1M_0) intercepts the surface at the point M_0, and that the sensor illuminates the point M_0. Like the zero-order case, the statistical illumination function, $S_1(\theta, \phi, \theta_1, \phi_1; \boldsymbol{\gamma}_0, \boldsymbol{\gamma}_1, z_0, z_1)$, can be averaged over the surface heights (z_0, z_1) defined at the points M_0 and M_1, corresponding to $\bar{S}_1(\theta, \phi; \theta_1, \phi_1; \boldsymbol{\gamma}_0, \boldsymbol{\gamma}_1)$ in Eq. (7). It will be derived in Section 3.

At the point M_0 with $\hat{\mathbf{m}}_1 = \overrightarrow{M_1M_0}$ and $\hat{\mathbf{m}}_0 = \overrightarrow{M_0M}$, the specular direction is defined as

$$\hat{\mathbf{m}}_1 = \hat{\mathbf{m}}_0 - 2(\hat{\mathbf{n}}_0 \cdot \hat{\mathbf{m}}_0)\hat{\mathbf{n}}_0 = \hat{\mathbf{m}}_0 - 2(\cos\psi_0)\hat{\mathbf{n}}_0, \quad (9)$$

where $\cos\psi_0$ is given by Eq. (2), and the normal vector to the facet at the point M_0 is $\hat{\mathbf{n}}_0 = (-\gamma_{x,0}, -\gamma_{y,0}, 1)/(1 + \gamma_{x,0}^2 + \gamma_{y,0}^2)^{1/2}$. In addition, with $i = \{0, 1\}$ in spherical coordinates, one has $\hat{\mathbf{m}}_i = (m_{x,i}, m_{y,i}, m_{z,i}) = (\cos\phi_i\sin\theta_i, \sin\phi_i\sin\theta_i, \cos\theta_i)$. Therefore from Eq. (2), Eq. (9) can be written as

$$\hat{\mathbf{m}}_1 = (m_{x,0} + G_0\gamma_{x,0}, m_{y,0} + G_0\gamma_{y,0}, m_{z,0} - G_0), \quad (10)$$

where

$$G_0 = \frac{2g_0 \cos\theta_0}{1 + \gamma_{x,0}^2 + \gamma_{y,0}^2} = \frac{2[\cos\theta_0 - (\gamma_{x,0}\cos\phi_0 + \gamma_{y,0}\sin\phi_0)\sin\theta_0]}{1 + \gamma_{x,0}^2 + \gamma_{y,0}^2}. \quad (11)$$

Thus the above equations allow us to calculate the components of the vector $\hat{\mathbf{m}}_1$ (or $\cos\theta_1 = m_{z,1}$ and $\tan\phi_1 = m_{y,1}/m_{x,1}$) with respect to the slopes $\{\gamma_{x,0}, \gamma_{y,0}\}$, and the angles $\{\theta_0 = \theta, \phi_0 = \phi\}$. Moreover, the angle ψ_1 is defined by using the same method as for ψ_0 given by Eq. (2), in which the subscript 0 is substituted for the subscript 1. Therefore in Eq. (7), the local emissivity depends only on the angles $\{\theta, \phi\}$ and the slopes $\{\gamma_{x,0}, \gamma_{y,0}, \gamma_{x,1}, \gamma_{y,1}\}$.

C. *N*-Order Emissivity

Using the same method as previously, the *N*-order average emissivity ($N > 0$), $\epsilon_N(\theta, \phi)$, is given by

$$\epsilon_N(\theta, \phi) = \langle[1 - |r(|\psi_N|)|^2] \times |r(|\psi_{N-1}|)|^2 \times \cdots \times |r(|\psi_0|)|^2 \times g_0 \times \bar{S}_N\rangle_N. \quad (12)$$

The *N*-order statistical illumination function, S_N gives the probability that the ray $(M_N M_{N-1})$ intercepts the surface at the point M_{N-1}, that the ray $(M_{N-1}M_{N-2})$ intercepts the surface at the point M_{N-2}, ..., that the ray $(M_1 M_0)$ intercepts the surface at the point M_0, and that the sensor illuminates the point M_0. Like the first-order case, the statistical illumination function, $S_N(\theta, \phi, \theta_1, \phi_1, \ldots, \theta_N, \phi_N; \boldsymbol{\gamma}_0, \boldsymbol{\gamma}_1, \ldots, \boldsymbol{\gamma}_N, z_0, z_1, \ldots z_N)$ can be averaged over the surface heights $\{z_0, z_1, \ldots, z_N\}$ defined at the points $\{M_0, M_1, \ldots, M_N\}$, corresponding to $\bar{S}_N(\theta, \phi, \theta_1, \phi_1, \ldots, \theta_N, \phi_N; \boldsymbol{\gamma}_0, \boldsymbol{\gamma}_1, \ldots, \boldsymbol{\gamma}_N)$ in Eq. (12). $\boldsymbol{\gamma}_n = [\gamma_{x,n} \quad \gamma_{y,n}]$ $(n = 0, \cdots, N)$, and ψ_n is the local angle between the normal to the facet, $\hat{\mathbf{n}}_n$, and the ray $(M_n M_{n-1})$. It is given by Eq. (2), in which the subscript 0 is substituted for the subscript *n*. The ensemble average operator $\langle \cdots \rangle_N$ is given by

$$\langle \cdots \rangle_N = \coprod_{n=0}^{n=N} \int_{-\infty}^{+\infty} (\cdots) p_s(\boldsymbol{\gamma}_n) \mathrm{d}\boldsymbol{\gamma}_n. \quad (13)$$

In addition, the components of $\hat{\mathbf{m}}_n = (m_{x,n}, m_{y,n}, m_{z,n})$ (or $\cos\theta_n = m_{z,n}$ and $\tan\phi_n = m_{y,n}/m_{x,n}$) are expressed from the ones of $\hat{\mathbf{m}}_{n-1}$ by using the same method as Eq. (10),

$$\hat{\mathbf{m}}_n = (m_{x,n-1} + G_{n-1}\gamma_{x,n-1}, m_{y,n-1} + G_{n-1}\gamma_{y,n-1}, m_{z,n-1} - G_{n-1}), \quad (14)$$

where G_{n-1} is expressed from Eq. (11), in which the subscript 0 is substituted for $n - 1$.

3. Illumination Function

A. Zero-Order Statistical Illumination Function

In this subsection, the zero-order statistical illumination function, S_0, is reviewed from Subsection 2.A of the paper of Bourlier[6] (for more details, see Refs. 12 and 13). It gives the probability that the point M_0 of height z_0 and slopes $\{\gamma_{x,0}, \gamma_{y,0}\}$ is illuminated by the sensor. It is given by

$$S_0[\theta, \phi; M_0(\gamma_{X,0}, z_0)] = F(z_0)^{\Lambda(\theta,\phi)}. \quad (15)$$

F is the cumulative function defined as

$$F(z_0) = \int_{-\infty}^{z_0} p_z(z)\mathrm{d}z, \quad (16)$$

in which p_z is the height PDF $[F(+\infty)=1]$. Equation (15) shows that the illumination function modifies the surface height due to the term $F(z_0)^\Lambda$ (it will also be shown that the illumination function carries a restriction over the surface slopes). Λ is given by

$$\Lambda(\theta, \phi) = \frac{1}{\mu}\int_{+\mu}^{+\infty} (\gamma_{X,0} - \mu) p_s(\gamma_{X,0})\mathrm{d}\gamma_{X,0}, \quad (17)$$

in which $\mu = |\cot\theta|$ is the slope of the incident beam along the azimuthal direction ϕ, and the slope marginal PDF $p_s(\gamma_{X,0})$ is expressed as

$$p_s(\gamma_{X,0}) = \int_{-\infty}^{+\infty} p_s(\gamma_{X,0}, \gamma_{Y,0})\mathrm{d}\gamma_{Y,0}, \quad (18)$$

where $\{\gamma_{X,0}, \gamma_{Y,0}\}$ are the surface slopes along the ϕ direction and the orthogonal direction, respectively, obtained from $\{\gamma_{x,0}, \gamma_{y,0}\}$ by executing a rotation of an angle ϕ,

$$\gamma_{X,0} = \gamma_{x,0}\cos\phi + \gamma_{y,0}\sin\phi, \quad \gamma_{Y,0} = -\gamma_{x,0}\sin\phi + \gamma_{y,0}\cos\phi. \quad (19)$$

For instance, for Gaussian statistics

$$p_s(\gamma_{x,0}, \gamma_{y,0}) = \frac{1}{2\pi\sigma_{sx}\sigma_{sy}} \exp\left(-\frac{\gamma_{x,0}^2}{2\sigma_{sx}^2} - \frac{\gamma_{y,0}^2}{2\sigma_{sy}^2}\right), \quad (20)$$

Eq. (18) becomes

$$p_s(\gamma_{X,0}) = \frac{1}{\sqrt{2\pi}\sigma_{sX}(\phi)} \exp\left[-\frac{\gamma_{X,0}^2}{2\sigma_{sX}^2(\phi)}\right],$$

where $\sigma_{sX}^2(\phi) = (\sigma_{sx}\cos\phi)^2 + (\sigma_{sy}\sin\phi)^2$ is the slope variance along the ϕ direction, and $\{\sigma_{sx}, \sigma_{sy}\}$ are the rms slope along the up and cross directions, respectively. In addition, from Eq. (17)

$$\Lambda(v) = \frac{\exp(-v^2) - v\sqrt{\pi}\,\mathrm{erfc}(v)}{2v\sqrt{\pi}}$$
$$v = v(\theta, \phi) = \frac{|\cot\theta|}{\sqrt{2}\sigma_{sX}(\phi)}. \quad (21)$$

Inasmuch as the zero-order local emissivity does not depend on the elevation z_0, one can average the zero-order statistical illumination function S_0 over the elevation z_0. From Eqs. (15) and (16), and for any height PDF p_z, one obtains

$$\overline{S}_0(\theta, \phi; \gamma_{X,0}) = \int_{-\infty}^{+\infty} S_0 p_z(z_0)\mathrm{d}z_0 = [1 + \Lambda(\theta, \phi)]^{-1}. \quad (22)$$

The zero-order statistical illumination function also carries a restriction over the surface slopes. Indeed, M_0 is illuminated by the sensor if the surface slope $\gamma_{X,0}$ along the direction ϕ is smaller than the ray slope of direction $\hat{\mathbf{m}}_0$, i. e., $\gamma_{X,0} \le \mu = |\cot\theta|$. Thus the substitution of Eqs. (22) and (19) into Eqs. (5) and (6) yields

$$\varepsilon_0(\theta,\phi) = [1 + \Lambda(\theta, \phi)]^{-1}\langle[1 - |r(|\psi_0|)|^2] \times g_0\rangle_0, \quad (23)$$

where

$$\langle\cdots\rangle_0 = \int_{-\infty}^{+\mu}\mathrm{d}\gamma_{X,0}\int_{-\infty}^{+\infty}(\cdots)p_s(\gamma_{X,0}, \gamma_{Y,0})\mathrm{d}\gamma_{Y,0}. \quad (24)$$

One can note that $\mathrm{d}\gamma_{x,0}\mathrm{d}\gamma_{y,0} = \mathrm{d}\gamma_{X,0}\mathrm{d}\gamma_{Y,0}$ (the Jacobian of the variable transformation is equal to 1).

For a sea surface with Gaussian and non-Gaussian statistics, numerical results of Eq. (23) with respect to the azimuthal direction ϕ, the emission angle θ, the wavelengths $\lambda = \{4, 10\}$ μm, and for moderate wind speeds, are reported in Ref. 6.

B. First-Order Statistical Illumination Function

The first-order statistical illumination function gives the probability that the ray (M_1M_0) intercepts the surface at the point M_0, and that the sensor illuminates the point M_0 (Fig. 1). It is expressed as[14]

$$S_1(\theta, \phi, \theta_1, \phi_1; M_1, M_0) = \tilde{S}_{0b}(\theta_1, \phi_1; M_1, M_0) \times S_{0b}(\theta, \phi; M_0, M). \quad (25)$$

$S_{0,b}(\theta_1, \phi_1; M_1, M_0)$ gives the probability that the ray (M_1M_0) emanating from the point M_1 of height z_1 and slopes $\{\gamma_{x,1}, \gamma_{y,1}\}$ does not intercept the surface at the point M_0 of height z_0 and slopes $\{\gamma_{x,0}, \gamma_{y,0}\}$, and $\tilde{S}_{0b} = 1 - S_{0b}$ is the complementary probability that gives the probability that the ray (M_1M_0) does intercept the surface at the point M_0. M is a point of the space with an infinite height. S_{0b} is expressed as

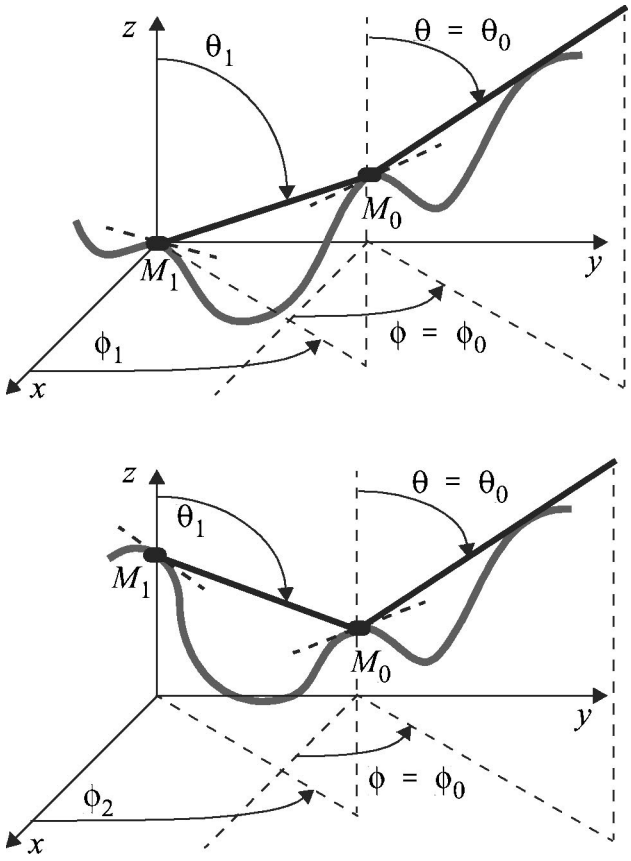

Fig. 2. Illustration of the first-order illumination function. At the top (upward case), $\theta_1 \in [0; \pi/2] \Rightarrow s = \mathrm{sgn}(\cos\theta_1) = +1$ and $z_1 \le z_0$. At the bottom (downward case), $\theta_1 \in [\pi/2; \pi] \Rightarrow s = \mathrm{sgn}(\cos\theta_1) = -1$ and $z_1 \ge z_0$. z_i stands for the height of the point M_i.

$$S_{0b}(\theta_1, \phi_1; M_1, M_0) = [F(z_1)/F(z_0)]^{s\Lambda_s(\theta_1,\phi_1)}$$
$$s = \mathrm{sign}(\cos\theta_1). \quad (26)$$

From Eq. (16), $F(+\infty) = 1$, and since the height of M is the infinity, $S_{0b}(\theta, \phi; M_0, M) = F(z_0)^{\Lambda_+(\theta,\phi)}$, which gives the probability that the point M_0 is viewed by the sensor, given by Eq. (15). According to the sign of $\cos\theta_1$ given by s (see Fig. 2), the ray (M_1M_0) goes either downward $(\theta_1 \in [\pi/2; \pi] \Rightarrow s = -1$ and $z_1 \ge z_0)$ or upward $(\theta_1 \in [0; \pi/2] \Rightarrow s = +1$ and $z_1 \le z_0)$. For the upward direction, the starting point is M_1, and $S_{0b}(\theta_1, \phi_1; M_1, M_0) = [F(z_1)/F(z_0)]^{\Lambda_+(\theta_1,\phi_1)}$, whereas for the downward direction, the starting point is M_0 and $S_{0b} = [F(z_0)/F(z_1)]^{\Lambda_-(\theta_1,\phi_1)} = [F(z_1)/F(z_0)]^{-\Lambda_-(\theta_1,\phi_1)} = S_{0b}(\theta_1, \phi_1; M_0, M_1)$. Thus S_{0b} of the upward direction is obtained from the one of the downward direction by changing M_1 with M_0.

For the upward direction, $\Lambda_+(\theta, \phi) = \Lambda(\theta, \phi)$ is given by Eq. (17), whereas for the downward direction, $\Lambda_-(\theta, \phi)$ is expressed as[15]

$$\Lambda_-(\theta, \phi) = \frac{1}{\mu}\int_{-\mu}^{+\infty}(\gamma_{X,0} + \mu)p_s(\gamma_{X,0})\mathrm{d}\gamma_{X,0} - 1. \quad (27)$$

One can show for an even slope marginal PDF $[p_s(-\gamma_{X,0}) = p_s(\gamma_{X,0})]$ that $\Lambda_+ = \Lambda = \Lambda_-$. This is why in Ref. 13, no distinction is made between Λ_+ and Λ_-, because the surface is supposed to be statistically even. One can note that this assumption holds for Gaussian statistics. The substitution of Eq. (26) into Eq. (25) leads to

$$S_1(\theta, \phi, \theta_1, \phi_1; M_1, M_0) = \left\{1 - \left[\frac{F(z_1)}{F(z_0)}\right]^{s\Lambda_s(\theta_1,\phi_1)}\right\} \times F(z_0)^{\Lambda(\theta,\phi)}. \quad (28)$$

The first-order average illumination function over the heights $\{z_1, z_0\}$, $\bar{S}_1(\theta, \phi, \theta_1, \phi_1)$, is defined by

$$\bar{S}_1(\theta, \phi, \theta_1, \phi_1) = \int_{-\infty}^{+\infty} p_x(z_0) \times \left[\int_{z_l{}^s}^{z_u{}^s} S_1(\theta, \phi, \theta_1, \phi_1; M_1, M_0) p_z(z_1)\right] dz_0, \quad (29)$$

where

$$z_u{}^+ = z_0 \quad z_l{}^+ = -\infty \quad \text{for } s = +1,$$
$$z_u{}^- = +\infty \quad z_l{}^- = z_0 \quad \text{for } s = -1. \quad (30)$$

For any surface statistics, after simple but tedious manipulations, the substitution of Eqs. (28) and (30) into Eq. (29) yields

$$\bar{S}_1(\theta, \phi, \theta_1, \phi_1) = \begin{cases} \Lambda_{1+}[(1 + \Lambda_{1+})(2 + \Lambda)]^{-1} & s = +1, \\ \Lambda_{1-}[(1 + \Lambda + \Lambda_{1-})(1 + \Lambda)(2 + \Lambda)^{-1}] & s = -1, \end{cases} \quad (31)$$

with $\Lambda = \Lambda(\theta, \phi)$ and $\Lambda_{1s} = \Lambda_s(\theta_1, \phi_1)$. For even statistics, for which $\Lambda = \Lambda_- = \Lambda_+ \geq 0$, the ratio $\bar{S}_{1+}/\bar{S}_{1-} \geq 1 \Rightarrow ½ \geq \bar{S}_{1+} \geq \bar{S}_{1-} \geq 0$. This result is consistent with the physical interpretation that $\bar{S}_{1+} \geq \bar{S}_{1-} \geq 0$ (see Fig. 2). The upper limit 1/2 is obtained for $\{\theta = 0, \theta_1 = \pi/2\} \Rightarrow \{\mu \to +\infty, \mu_1 = 0\} \Rightarrow \{\Lambda = 0, \Lambda_{1\pm} \to +\infty\}$, and comes from the fact that only the heights $z_1 \geq z_0$ (the case where $s = -1$) or $z_0 \geq z_1$ (the case where $s = +1$) contribute in the calculation of the average illumination function.

Like the zero-order case, the first-order statistical illumination function carries a restriction over the surface slopes. Indeed, as depicted in Fig. 2, the point M_0 is viewed by the sensor if the slope of the ray emanating from M_0, μ, is greater than the surface slope, $\gamma_{X,0}$, at the point M_0 along the azimuthal direction ϕ. It is derived from Eq. (19). Using the same approach for $\theta_1 \in [0; \pi/2]$ $(s = +1)$, M_1 is viewed from M_0 if the slope of the ray (M_1M_0), $\mu_1 = |\cot \theta_1|$, is greater than $\gamma_{X,1}$. For $\theta_1 \in [\pi/2; \pi]$ $(s = -1)$, this condition becomes $\gamma_{X,1} \geq -\mu_1 = s\mu_1$. Thus the first-order average emissivity is given by Eq. (7), in which $\bar{S}_1$ is given by Eq. (31). In addition, the ensemble average expressed from Eq. (8) becomes

$$\langle \cdots \rangle_1 = \int_{-\infty}^{+\mu} \int_{\gamma_{1l}}^{\gamma_{1u}} \int_{-\infty}^{+\infty} \int_{-\infty}^{+\infty} (\cdots) p_s(\Gamma_0) p_s(\Gamma_1) \times d\gamma_{Y,1} d\gamma_{Y,0} d\gamma_{X,1} d\gamma_{X,0}, \quad (32)$$

where $\mathbf{\Gamma}_i = [\gamma_{X,i}, \gamma_{Y,i}]$ with $i = \{0, 1\}$, and the restriction over the slopes $\{\gamma_{X,0}, \gamma_{X,1}\}$ is absorbed in the limits of integrations. Indeed, for $s = +1$, $\{\gamma_{1l} = -\infty, \gamma_{1u} = \mu_1\}$, whereas for $s = -1$, $\{\gamma_{1l} = -\mu_1, \gamma_{1u} = +\infty\}$ with $\mu_1 = |\cot \theta_1|$. From Eq. (19), one can note that $d\gamma_{x,0} d\gamma_{y,0} d\gamma_{x,1} d\gamma_{y,1} = d\gamma_{X,0} d\gamma_{Y,0} d\gamma_{X,1} d\gamma_{Y,1}$ (the Jacobian of the variable transformation is equal to 1).

C. *N*-Order Statistical Illumination Function

Using the same method as previously, the *N*-order statistical illumination function is expressed as

$$S_N(\mathbf{\Phi}, \mathbf{\Theta}; \mathbf{Z}, \mathbf{\Gamma}_X) = S_{0b}(\theta, \phi; M_0, M) \Upsilon(\mu - \gamma_{X,0}) \times \prod_{n=1}^{n=N} \Upsilon(\mu_n - s_n \gamma_{X,n}) \times \widetilde{S}_{0b}(\theta_n, \phi_n; M_{n-1}, M_n), \quad (33)$$

where $\mathbf{\Theta} = [\theta, \theta_1, \ldots, \theta_N]$, $\mathbf{\Phi} = [\phi, \phi_1, \ldots, \phi_N]$, $\mathbf{Z} = [z_0, z_1, \ldots, z_N]$, $\mathbf{\Gamma}_X = [\gamma_{,0}, \gamma_{X,1}, \ldots, \gamma_{X,N}]$, and $s_n = \text{sign}(\cos \theta_n)$ $(\theta = \theta_0, \phi = \phi_0, \mu_0 = \mu)$. $\Upsilon(x) = 1$ if $x \geq 0$, 0 otherwise and corresponds to the restriction over the surface slopes. The average illumination function over the heights $\mathbf{Z}$ is then defined by

$$\widetilde{S}_N(\mathbf{\Phi}, \mathbf{\Theta}; \mathbf{\Gamma}_X) = \bar{S}_N(\mathbf{\Phi}, \mathbf{\Theta}) \prod_{n=0}^{n=N} \Upsilon(\mu_n - s_n \gamma_{X,n}), \quad (34)$$

where

$$\bar{S}_N(\mathbf{\Phi}, \mathbf{\Theta}) = \int_{-\infty}^{+\infty} p_z(z_0) \int_{z_{l,1}{}^{s_1}}^{z_{u,1}{}^{s_1}} p_z(z_1) \cdots \int_{z_{l,N}{}^{s_N}}^{z_{u,N}{}^{s_N}} p_z(z_N) \times [F(z_0)]^{\Lambda(\theta,\phi)} \prod_{n=1}^{n=N} \left\{1 - \left[\frac{F(z_n)}{F(z_{n-1})}\right]^{\theta_n \Lambda_{s_n}(\theta_n,\phi_n)}\right\} dz_0 dz_1, \ldots, dz_N, \quad (35)$$

and

$$z_{u,n}{}^+ = z_{n-1} \quad z_{l,n}{}^+ = -\infty \quad \text{for } s_n = +1,$$
$$z_{u,n}{}^- = +\infty \quad z_{l,n}{}^- = z_{n-1} \quad \text{for } s_n = -1. \quad (36)$$

For instance, for $N = 2$, after simple but tedious manipulations, the second-order average illumination function $\bar{S}_2(\theta, \phi, \theta_1, \phi_1, \theta_2, \phi_2)$ is expressed as

$$\begin{array}{ll} \dfrac{\Lambda_{1+}\Lambda_{2+}}{2(3+\Lambda)(2+\Lambda_{1+})(1+\Lambda_{2+})} & s_1 = +1 \quad s_2 = +1, \\ \tilde{\bar{S}}_2 + \lim\limits_{\substack{\Lambda_{1+}\to+\infty \\ \Lambda_{2-}\to+\infty}} \tilde{\bar{S}}_2 - \lim\limits_{\Lambda_{1+}\to+\infty} \tilde{\bar{S}}_2 - \lim\limits_{\Lambda_{2-}\to+\infty} \tilde{\bar{S}}_2 & s_1 = +1 \quad s_2 = -1, \\ \dfrac{\Lambda_{1-}\Lambda_{2+}}{(1+\Lambda)(3+\Lambda)(1+\Lambda+\Lambda_{1-})(1+\Lambda_{2+})} & s_1 = -1 \quad s_2 = +1, \\ \dfrac{\Lambda_{1-}\Lambda_{2-}}{(1+\Lambda)(2+\Lambda)(3+\Lambda)(1+\Lambda+\Lambda_{1-})(2+\Lambda+\Lambda_{2-})} & s_1 = -1 \quad s_2 = -1. \end{array} \tag{37}$$

For the case $\{s_1 = +1, s_2 = -1\}$, the illumination function is split up into as $(1 - F_{10}^{\Lambda_{1+}})(1 - F_{21}^{\Lambda_{2-}}) = F_{10}^{\Lambda_{1+}} F_{21}^{\Lambda_{2-}} + 1 - F_{10}^{\Lambda_{1+}} - F_{21}^{\Lambda_{2-}}$, where $F_{ij} = F(z_i)/F(z_j)$, because the final expression is not simple. $\tilde{\bar{S}}_2$ corresponds then to the statistical average of $F_{10}^{\Lambda_{1+}} F_{21}^{\Lambda_{2-}}$ given by

$$\tilde{\bar{S}}_2 = \frac{4 + \Lambda + \Lambda_{1+} + \Lambda_{2-}}{(3+\Lambda)(2+\Lambda_{1+})(2+\Lambda+\Lambda_{2-})(1+\Lambda_{1+}+\Lambda_{2-})}. \tag{38}$$

For $\theta_1 = \theta_2 = \pi/2 \Rightarrow \Lambda_1 \to \Lambda_2 \to +\infty$ [the probability that the rays (M_2M_1) and (M_1M_0) emanating from the points $\{M_2, M_1\}$ intercept the surface at the points $\{M_1, M_0\}$, respectively, is very strong] with even statistics and $\theta = 0$ (no shadowing), one has $\bar{S}_2 = \left\{\frac{1}{6}, \frac{1}{3}, \frac{1}{3}, \frac{1}{6}\right\}$ for $(s_1, s_2) = \{(+1+1), (+1-1), (-1+1), (-1-1)\}$. One can then observe that the sum of $\bar{S}_2$ over (s_1, s_2) is equal to 1 like the case where $N = 1$.

The N-order emissivity is then expressed from Eq. (12), in which $\bar{S}_N$ is given by Eq. (35) and the ensemble average operator, expressed from Eq. (13), becomes

$$\langle \cdots \rangle_N = \prod_{n=0}^{n=N} \int_{-\infty}^{+\infty} \int_{-\infty}^{+\infty} (\cdots) p_s(\gamma_{X,n}, \gamma_{Y,n}) \times \Upsilon(\mu_n - s_n \gamma_{X,n}) \mathrm{d}\gamma_{X,n} \mathrm{d}\gamma_{Y,n}. \tag{39}$$

4. Numerical Results

From Eqs. (12) and (39), the N-order emissivity requires the computation of $2(N+1)$- fold numerical integrations over the surface slopes $\mathbf{\Gamma}_n = [\gamma_{X,n}\ \gamma_{Y,n}]$ $(n = 0, \cdots N)$. The purpose of this paper is to study the contribution of the multiple reflections, which does not much depend on the anisotropy of the surface. Thus to reduce the number of integrations, the rough surface is assumed to be 1D (in Ref. 6 and for $N = 0$, a detailed study with respect to the azimuthal wind direction ϕ is reported for Gaussian and non-Gaussian statistics, for moderate wind speeds, and in the infrared near band). In addition, in this paper, a rough sea surface with Gaussian statistics, $p_s(\gamma) = (1/\sqrt{2\pi}\sigma_s)\exp[-(\gamma^2/2\sigma_s^2)]$, is considered. The emissivity is computed in the infrared near band by considering wavelengths $\lambda = \{4, 10\}\ \mu$m, and the corresponding sea refraction index is given by Hale and Querry,[16] $n_{\mathrm{sea}} = \{1.3510 + 0.0046i, 1.2180 + 0.0508i\}$, in which the sea is assumed to be a pure water (no salt). The wind speeds, u_{12}, defined at 12.5 m above the sea, are chosen as $\{5, 10, 15, 20\ \mathrm{m/s}\}$ corresponding to rms slopes equal to $\sigma_s = \{0.126, 0.178, 0.218, 0.251\}$ from the Cox–Munk[17] model ($\sigma_s = 0.0562\sqrt{u_{12}}$ along the wind direction).

A. Emissivities for a One-Dimensional Random Rough Surface

For a 1D rough sea surface, $\phi_n = 0$, and the surface slope $\gamma_n = [\gamma_{x,n}\ \ \gamma_{y,n}]$ at the point M_n becomes scalar $\gamma_n = \gamma_{x,n} \equiv \gamma_n$. In addition, from Eq. (19), $\gamma_{X,n} = \gamma_n$ and $\gamma_{Y,n} = 0$. From Eqs. (23) and (24), the zero-order emissivity is

$$\varepsilon_0(\theta) = \frac{1}{1+\Lambda(\theta)} \int_{-\infty}^{+\mu} [1 - |r(|\psi_0|)|^2] p_s(\gamma_0) g_0 \mathrm{d}\gamma_0, \tag{40}$$

in which [Eqs. (2) and (4)]

$$g_0 = 1 - \gamma_0 \tan\theta_0, \tag{41}$$

and

$$\cos[\psi_0(\theta_0; \gamma_0)] = g_0 \cos\theta_0 (1 + \gamma_0^2)^{-1/2}. \tag{42}$$

For Gaussian statistics, $\Lambda(\theta)$ is expressed from Eq. (17), in which $v(\theta) = |\cot\theta|/(\sqrt{2}\sigma_s)$ with σ_s the surface rms slope.

From Eqs. (7) and (32), the first-order average

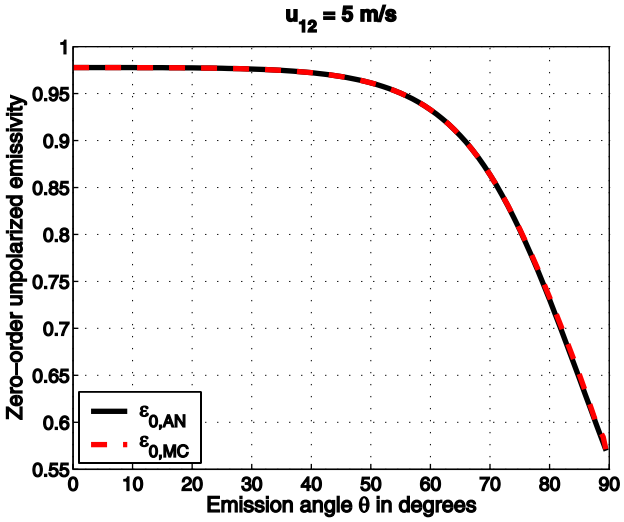

Fig. 3. (Color online) Zero-order emissivities $\varepsilon_{0,AN}$ and $\varepsilon_{0,MC}$ computed from an analytical approach [(Eq. 40)] and a Monte Carlo ray-tracing method versus the emission angle θ. The wind speed $u_{12} = 5$ m/s and the wavelength $\lambda = 4$ μm.

emissivity is

$$\varepsilon_1(\theta) = \int_{-\infty}^{+\mu} d\gamma_0 \int_{\gamma_{1l}}^{\gamma_{1u}} [1 - |r(|\psi_1|)|^2] \times |r(|\psi_0|)|^2 \bar{S}_1(\theta_1, \theta_2) p_s(\gamma_1) p_s(\gamma_0) g_0 d\gamma_1. \quad (43)$$

The first-order average illumination function $\bar{S}_1(\theta_1, \theta_2)$ is given by Eq. (31). For Gaussian statistics, $\Lambda_{n+} = \Lambda_{n-} = \Lambda(\theta_n)$ $(n = 0, \cdots, N)$. For $s = +1$, $(\gamma_{1l} = -\infty, \gamma_{2u} = \mu_1)$, whereas for $s = -1$, $\{\gamma_{1l} = -\mu_1, \gamma_{1u} = +\infty\}$ with $\mu_1 = |\cot \theta_1|$. From Eqs. (10) and (11), one has $m_{z,1} = m_{z,0} - G_0$, leading to

$$\cos \theta_1 = \cos \theta_0 \left[1 - 2g_0 (1 + \gamma_0^2)^{-1}\right]. \quad (44)$$

In addition, $\cos \psi_1$ is given by Eq. (42), in which the subscript 0 is substituted for the subscript 1.

For the second-order emissivity, $\varepsilon_2(\theta)$, one obtains from Eqs. (12) and (35) a similar expression

$$\varepsilon_2(\theta) = \int_{-\infty}^{+\mu} d\gamma_0 \int_{\gamma_{1l}}^{\gamma_{1u}} d\gamma_1 \int_{\gamma_{2l}}^{\gamma_{2u}} [1 - |r(|\psi_2|)|^2] \times |r(|\psi_1|)|^2 |r(|\psi_0|)|^2 \times \bar{S}_2(\theta, \theta_1, \theta_2) p_s(\gamma_2) p_s(\gamma_1) p_s(\gamma_0) g_0 d\gamma_2, \quad (45)$$

in which

$$\cos \theta_2 = \cos \theta_1 \left[1 - 2g_0 (1 + \gamma_0^2)^{-1}\right]\left[1 - 2g_1 (1 + \gamma_1^2)^{-1}\right], \quad (46)$$

and $\bar{S}_2(\theta, \theta_1, \theta_2)$ is expressed from Eqs. (37) and (38).

B. Simulations of the Emissivities

In Fig. 3, the zero-order emissivity $\varepsilon_{0,AN}$ derived from an analytical approach [Eq. (40)] is plotted versus the emission angle θ. The wind speed $u_{12} = 5$ m/s and the wavelength $\lambda = 4$ μm. In addition, this approach is compared with a benchmark approach based on a Monte Carlo ($\varepsilon_{0,MO}$) ray tracing method:

1. The surface height samples, $z(i)$, are computed from $z(i) = \mathcal{F}^{-1}[\tilde{b}(i)\sqrt{\tilde{\omega}(i)}]$, in which $\tilde{b}(i)$ is a Gaussian white noise in the Fourier domain with zero mean value and unit standard deviation, and $\tilde{\omega}(i)$ the surface height spectral density, assumed to be Gaussian, $\tilde{\omega}(i) = \sigma_h^2 L_c \sqrt{\pi} \exp(-\pi^2 i^2 L_c^2)$, where L_c is the surface height correlation length and σ_h the surface rms height (see Ref. 12 for more details). The slopes $\gamma(i) = [z(i+1) - z(i)]/\Delta x$, where Δx is the sampling step.
2. From $z(i)$, the illumination function is computed for each order. For the zero order, the method is explained in detail in Ref. 12; only the indexes $i = i_0$ of the surface points illuminated by the sensor are taken into account in the calculation of the statistical average. In other words, for the computation of the statistical averaging over the surface heights and slopes, one takes into account only $z(i_0)$ and $\gamma(i_0)$. For the first order, using the algorithm that calculates the zero-order illumination function, only the surface points illuminated by the sensor are kept [corresponding to the point M_0 of height $z(i_0) = z_0$ and slope $\gamma(i_0) = \gamma_0$]; these points are kept if the rays emanating from these points with an incidence angle $\theta_1(\gamma_0)$ given by Eq. (44) intercept the surface [corresponding to the point M_1 of height $z(i_1) = z_1$ and slope $\gamma(i_1) = \gamma_1$, where i_1 is the sample index]. For the N-order illumination function, one repeats the procedure to obtain $\{z(i_0) = z_0, z(i_1) = z_1, \ldots, z(i_N) = z_N\} \equiv \mathbf{Z}$ and $\{\gamma(i_0) = \gamma_0, \gamma(i_1) = \gamma_1, \ldots, \gamma(i_N) = \gamma_N\} \equiv \boldsymbol{\gamma}$.
3. From $\mathbf{Z}$ and $\boldsymbol{\gamma}$, the local emissivity is computed for each order. For the zero order, from Eqs. (40) and (41) one has $\epsilon_{l0} = \left[1 - |r(|\psi_0|)|^2\right] g_0$, in which $\gamma_0 = \gamma(i_0)$ and $\psi_0(\theta_0; \gamma_0)$ is given by Eq. (42). For the first order, from Eq. (43), the first-order local emissivity is $\left[1 - |r(|\psi_1|)|^2\right] |r(|\psi_0|)|^2 g_0$, where ψ_i is given by Eq. (42) with $\gamma_i = \gamma(i)$ $(i = \{0, 1\})$, and so on.
4. For each order, the average emissivity, $\varepsilon_n(\theta)$, is computed as $\varepsilon_n(\theta) = (1/N_s) \sum_{i=1}^{i=N_s} \varepsilon_{ln} \delta_{i,i_n}$, where N_s is the number of surface samples, and $\delta_{i,j}$ is the Kronecker symbol defined as $\delta_{i,j} = 1$ (the point is illuminated) if $i = j$, 0 otherwise (the point is shaded).
5. To obtain a good convergence of the method (i.e., the surface statistics are well reproduced), steps 1, 2, 3, and 4 are repeated N_r times.

$N_s = 20{,}000$ for each surface height sample $z(i)$, which are statistically independent, and the surface correlation length $L_c = 100$. The N-order average emissivity is calculated from each surface and for a number of realizations of $N_r = 100$.

In Fig. 3, very good agreement is observed between both methods, which means that the model is accurate to derive the zero-order illumination function. As shown by Bourlier[6] from the Monte Carlo results,[11]

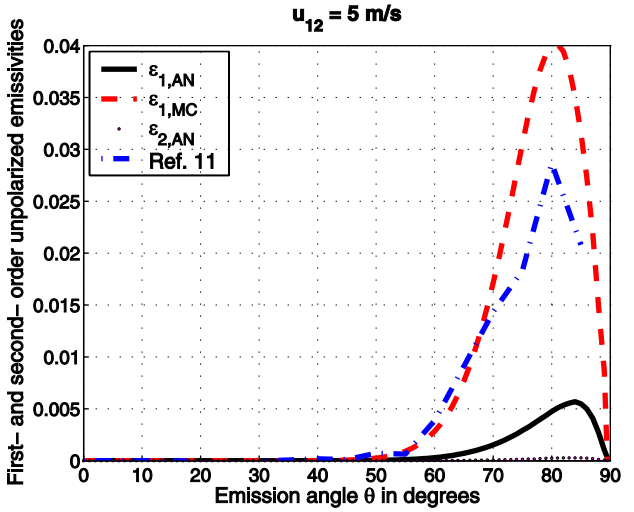

Fig. 4. (Color online) First- and second-order emissivities $\{\varepsilon_{1,AN}, \varepsilon_{2,AN}, \varepsilon_{1,MC}\}$ computed from analytical approaches [Eqs. (43) and (45)] and from a Monte Carlo method versus the emission angle θ. The results of Ref. 11 are also plotted. The wind speed $u_{12} = 5$ m/s and the wavelength $\lambda = 4$ μm.

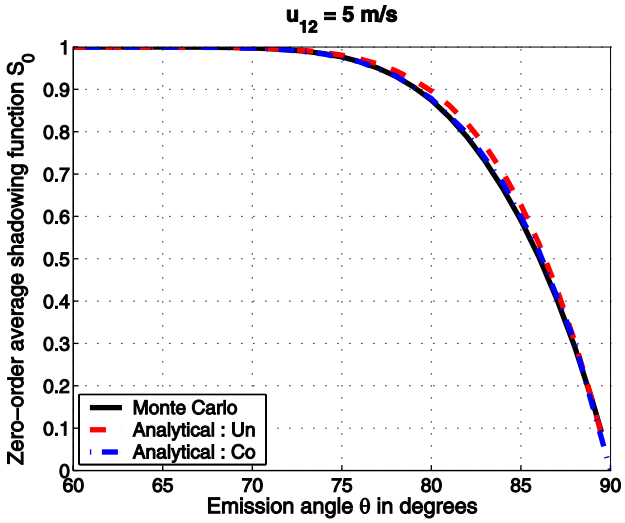

Fig. 5. (Color online) Zero-order average illumination function $\bar{\bar{S}}_0(\theta)$ computed from a Monte Carlo method, from Eq. (48) (without correlation) and when the correlation is taken into account versus the emission angle θ. The wind speed $u_{12} = 5$ m/s.

this remark also holds for 2D rough anisotropic sea surfaces.

In Fig. 4, the first- and second-order emissivities $\{\varepsilon_{1,AN}, \varepsilon_{2,AN}, \varepsilon_{1,MC}\}$ computed from analytical approaches [Eqs. (43) and (45)] and from a Monte Carlo method are compared versus the emission angle θ. The wind speed $u_{12} = 5$ m/s and the wavelength $\lambda = 4$ μm. The results of Henderson, Theiler, and Villeneuve are also plotted. They considered a Gaussian 2D anisotropic sea surface, a wind direction $\phi = 0$ (the rms slope is then given by $\sigma_s = 0.056\sqrt{u_{12}}$), the multiple reflections are taken into account up to the order 10, and the emission angle ranges from 0° to 85° in steps of 5°. One can observe that the contribution of $\varepsilon_{2,AN}$ is 20 times smaller than the one of $\varepsilon_{1,AN}$. Unlike ε_0, a strong disagreement of ε_1 is observed between the analytical and the Monte Carlo results. The results of ε_1 computed from a Monte Carlo method are consistent with the ones of Ref. 11.

C. Simulations of the Illumination Functions

To understand the disagreement between $\varepsilon_{1,AN}$ and $\varepsilon_{1,MC}$, the zero-($\bar{\bar{S}}_0$) order and first-($\bar{\bar{S}}_1$) average illumination functions over the heights and slopes are calculated and compared with the ones obtained from a Monte Carlo method (over S_0 and S_1, the first bar corresponds to the averaging over the surface slopes, and the second bar corresponds to the averaging over the surface heights). Indeed, the only difference between $\varepsilon_{n,MC}$ and $\varepsilon_{n,AN}$ is in the calculation of the n-order illumination function (the n-order local emissivities without shadow are the same).

The zero-order average illumination function, $\bar{\bar{S}}_0(\theta)$, averaged over the heights, z_0, and over the slopes, γ_0, at the point M_0 is defined as

$$\bar{\bar{S}}_0(\theta) = \left\{\int_{-\infty}^{+\infty} [F(z_0)]^{\Lambda} p_z(z_0)\mathrm{d}z_0\right\}\int_{-\infty}^{+\mu} p_s(\gamma_0)\mathrm{d}\gamma_0 = \frac{1}{1+\Lambda}\int_{-\infty}^{+\mu} p_s(\gamma_0)\mathrm{d}\gamma_0. \quad (47)$$

For Gaussian statistics, the above equation becomes

$$\bar{\bar{S}}_0(\theta) = [1 + \mathrm{erf}(v)]\{2[1 + \Lambda(v)]\}^{-1}. \quad (48)$$

In Fig. 5, $\bar{\bar{S}}_0(\theta)$ computed from a Monte Carlo method and from Eq. (48) is plotted versus the emission angle θ and for a wind speed $u_{12} = 5$ m/s. The Monte Carlo method is based on the steps 1 and 2 of Subsection 4.B. For instance, for the zero order, from the knowledge of $\{i_0\}$, corresponding to the indexes of the surface points illuminated by the sensor, the zero-order average illumination function is then $(1/N_s)\sum_{i=1}^{i=N_s}\delta_{i,i_0} \leq 1$, where $\delta_{i,i} = 1$, 0 otherwise ($i \neq j$). The n-order average illumination function is $(1/N_s)\sum_{i=1}^{i=N_s}\delta_{i,i_n}$. $\bar{\bar{S}}_0(\theta)$ with correlation[12] is also plotted. A good agreement among the three methods is observed, and one can see that $\bar{\bar{S}}_0(\theta)$ computed from the analytical method without correlation is slightly overestimated. When the correlation is taken into account, this overestimation decreases. This explains in Fig. 3 that a very good agreement is obtained for the zero-order emissivity.

The first-order average illumination function, $\bar{\bar{S}}_1(\theta)$, averaged over the heights $\{z_0, z_1\}$, and over the slopes $\{\gamma_0, \gamma_1\}$, at the points $\{M_0, M_1\}$ is expressed as

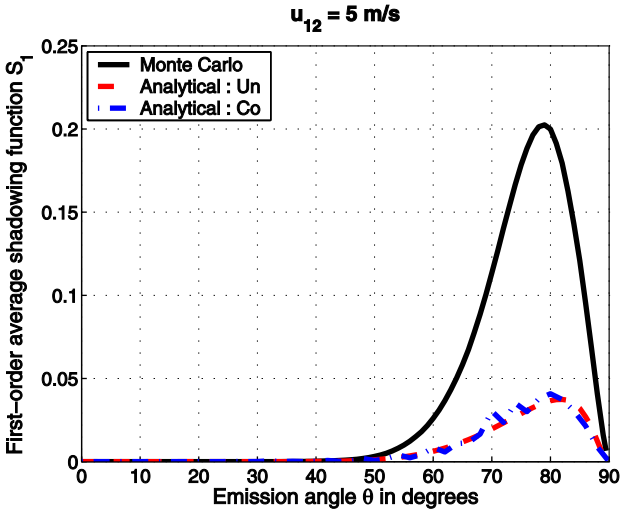

Fig. 6. (Color online) First-order average illumination function $\bar{\bar{S}}_1(\theta)$ computed from a Monte Carlo method, from Eq. (50) (without correlation) and when the correlation is taken into account versus the emission angle θ. The wind speed $u_{12} = 5$ m/s.

$$\bar{\bar{S}}_1(\theta) = \int_{-\infty}^{+\infty}\int_{-\infty}^{+\infty} \bar{S}_1(\theta,\theta_1)\Upsilon(\mu - \gamma_0) \times \Upsilon(\mu_1 - s\gamma_1)p_s(\gamma_0)p_s(\gamma_1)\mathrm{d}\gamma_0\mathrm{d}\gamma_1, \quad (49)$$

where $\bar{S}_1(\theta, \theta_1)$ is given by Eq. (31), in which θ_1 depends on $\{\theta, \gamma_1\}$ within Eq. (44). For Gaussian statistics, $p_s(\gamma) = (1/\sqrt{2\pi\sigma_s})\exp[-(\gamma^2/2{\sigma_s}^2)]$, the integration over γ_1 leads to

$$\bar{\bar{S}}_1(\theta) = \frac{1}{2\sqrt{2\pi\sigma_s}}\int_{-\infty}^{+\mu} \bar{S}_1[\theta,\, \theta_1(\gamma_0)][1 + \mathrm{erf}(v_1)] \times \exp\left(-\frac{{\gamma_0}^2}{2{\sigma_s}^2}\right)\mathrm{d}\gamma_0. \quad (50)$$

$\bar{\bar{S}}_1(\theta)$ is also computed from a Monte Carlo method: Applying steps 1 and 2 of Subsection 4.B, from the knowledge of $\{i_1\}$ (corresponding to the indexes of the surface points M_1 illuminated by the points M_0, which is illuminated by the sensor), the first-order average illumination function is then $(1/N_s)\sum_{i=1}^{i=N_s}\delta_{i,i_1} \leq 1$. Like $\bar{\bar{S}}_0(\theta)$, $\bar{\bar{S}}_1(\theta)$ is calculated when the statistical correlation between the points M_1 and M_0 is taken into account. It is given by

$$\bar{\bar{S}}_1(\theta) = \int_{-\infty}^{+\mu}\mathrm{d}\gamma_0\int_{-\infty}^{+\infty}\mathrm{d}\gamma_1\int_{-\infty}^{+\infty}\mathrm{d}z_0\int_{{z_l}^s}^{{z_u}^s}\mathrm{d}z_1 \times [1 - S_{0b}(\theta_1; M_1, M_0)]S_{0b}(\theta; M_1, M_0 \to \infty) \times \Upsilon(\mu_1 - s\gamma_1)p_z(z_0)p_z(z_1)p_s(\gamma_0)p_s(\gamma_1). \quad (51)$$

For Gaussian surface statistics, the details of the calculation of $S_{0b}(\theta_1; M_1, M_0)$ with correlation are reiterated in the appendix. Unlike the uncorrelated case, for the downward direction $S_{0b}(\theta_1; M_1, M_0)$ depends on the slope γ_1, which implies that the integration over γ_1 cannot be derived analytically. On the other hand, the integration over γ_0 with Gaussian statistics leads to $[1 + \mathrm{erf}(v)]/2$. For the upward direction, the points $\{M_0, M_1\}$ are substituted for the points $\{M_1, M_0\}$, which implies that the integration over γ_1 with Gaussian statistics gives $[1 + \mathrm{erf}(v_1)]/2$, whereas the integration over the slope γ_0 is computed numerically. In both cases, the integrations over the heights z_0 and z_1 are made numerically, unlike in the uncorrelated case. In conclusion, four numerical integrations $\{z_0, z_1, \gamma_{0,1}, u\}$ are needed to calculate $\bar{\bar{S}}_1(\theta)$.

In Fig. 6, $\bar{\bar{S}}_1(\theta)$ computed from a Monte Carlo method and from Eq. (50) is plotted versus the emission angle θ. The wind speed $u_{12} = 5$ m/s. $\bar{\bar{S}}_1(\theta)$ with correlation given by the above equation is also plotted. A disagreement between the Monte Carlo method and the analytical approaches is observed. This shows that the disagreement observed in Fig. 4 is because the calculation of the first-order illumination function is incorrect.

Other simulations of Figs. 3–6 obtained for wind speeds ranging from 5 to 20 m/s and not reported in this paper lead to the same conclusion.

D. Discussion and Description of the Empirical Approach

In this section, an empirical approach is proposed to obtain better agreement between the Monte Carlo and the analytical results of the first-order emissivity.

From Figs. 3 and 5, one can conclude that the analytical approach used to derive the zero-order illumination function is correct. The first-order statistical illumination function is expressed from Eq. (25), in which $S_{0b}(\theta,\phi; M_0, M)$ corresponds to the zero-order statistical illumination function. Thus the fact that S_1 is underestimated is because in Eq. (25), $\widetilde{S}_{0b}(\theta_1, \phi_1; M_1, M_0)$ is underestimated since $S_{0b}(\theta, \phi; M_0, M) = F(z_0)^{\Lambda}$ can be considered as being correct (Figs. 3 and 5). In addition, $\widetilde{S}_{0b}(\theta_1, \phi_1; M_1, M_0) = 1 - S_{0b}(\theta_1, \phi_1; M_1, M_0)$, in which S_{0b} is expressed from Eq. (26). Consequently, $S_{0b}(\theta_1, \phi_1; M_1, M_0)$ is overestimated. To diminish this quantity, several attempts have been studied: multiplying Eq. (26) by a constant $a \in |0; 1|$; multiplying Eq. (26) by $a^{\Lambda_s}(\Lambda_s \geq 0)$, $a^{\Lambda_1}(\Lambda_1 \geq 0)$, and $a^{\Lambda_s+\Lambda_1}$; substituting Λ_s in Eq. (26) for $b\Lambda_s$ with $b > 1$. Indeed, since the ratio $0 \leq F(z_1)/F(z_0) \leq 1 \Rightarrow [F(z_1)/F(z_0)]^{b\Lambda_s} < [F(z_1)/F(z_0)]^{\Lambda_s}$. Unfortunately, this led to no success.

Rigorously, $S_{0b}(\theta_1, \phi_1; M_1, M_0)$ is expressed from infinite series of Rice,[12] in which $2P$ integrations are involved, where P is the truncating order of the sum. Bourlier *et al.*[12] showed for any *uncorrelated* process that these integrations can be done analytically. Unfortunately, this approximation leads to an overestimation of the average illumination function. If the *correlation* is taken into account, the problem can be solve analytically only for $P = 1$ and by assuming

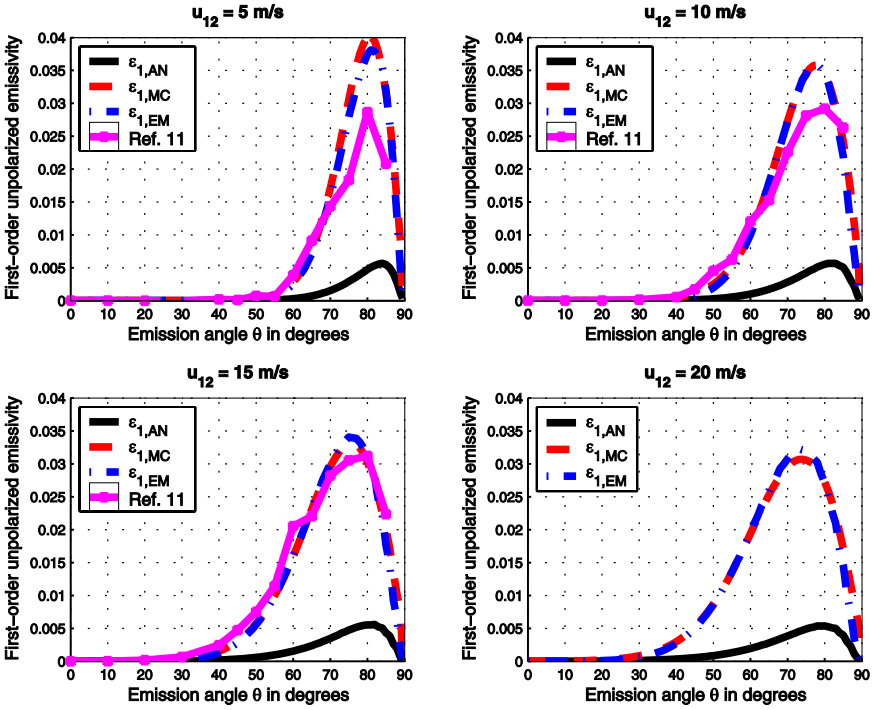

Fig. 7. (Color online) First-order emissivities computed from analytical $\varepsilon_{1,\mathrm{AN}}$, Monte Carlo $\varepsilon_{1,\mathrm{MC}}$ and empirical $\varepsilon_{1,\mathrm{EM}}$ approaches versus the emission angle θ. The results of Ref. 11 are also reported. The wind speeds $u_{12} = \{5, 10, 15, 20\}$ m/s and the wavelength $\lambda = 4$ μm.

Gaussian statistics (this corresponds to the illumination function with correlation). Thus it is proposed to correct the first-order emissivity computed from the analytical approach, $\varepsilon_{1,\mathrm{AN}}$, from an empirical function f defined as

$$f(\theta) = A \exp\left[-\frac{(\theta - m_1)^2}{\sigma_1^{\,2}}\right]. \tag{52}$$

The empirical first-order emissivity, $\varepsilon_{1,\mathrm{EM}}$, is then defined from $\varepsilon_{1,\mathrm{AN}}$ as

$$\varepsilon_{1,\mathrm{EM}} = f \times \varepsilon_{1,\mathrm{AN}}. \tag{53}$$

In addition, $\{A, m_1, \sigma_1\}$ are calculated from the ratio $R_{\varepsilon_1} = \varepsilon_{1,\mathrm{MC}}/\varepsilon_{1,\mathrm{AN}}$, where $\varepsilon_{1,\mathrm{MC}}$ is the emissivity calculated from the Monte Carlo method. From $R_{\varepsilon_1}(\theta)$ defined for $\theta \in [40; 85]$ degrees, A is computed by taking the maximum value of R_{ε_1}, m_1 is equal to the emission angle that gives A, and σ_1 is calculated from the emission angle θ_{10} for which $R_{\varepsilon_1}(\theta_{10})/A = 0.6 \Rightarrow \sigma_1 = (\theta_{10} - m_1)\sqrt{-1/\ln(0.6)}$.

In Fig. 7, the first-order emissivities ε_1 computed from analytical ($\varepsilon_{1,\mathrm{AN}}$), Monte Carlo ($\varepsilon_{1,\mathrm{MC}}$) and empirical ($\varepsilon_{1,\mathrm{EM}}$) approaches are plotted versus the emission angle θ. The wind speeds $u_{12} = \{5, 10, 15, 20\}$ m/s and the wavelength $\lambda = 4$ μm. For $u_{12} = \{5, 10, 15\}$ m/s, the results of Ref. 11 are also reported. One observes a good agreement between the empirical and the Monte Carlo results, which means that the choice of f is good. Similar simulations obtained for $\lambda = 10$ μm lead to the same conclusion. As the wind speed increases, the angular repartition of $\varepsilon_{1,\mathrm{MC}}$ is wider because the surface is rougher, and thus the surface scatters energy in a wider angular lobe. On the other hand, the maximum of $\varepsilon_{1,\mathrm{MC}}$ varies very slightly when the wind speed increases. One notes that the numerical results computed from a Monte Carlo method are consistent with the ones of Ref. 11, in which the multiple reflections are taken into account up to order 10. Therefore one can conclude that the contributions of orders larger than 1 are negligible. This is in agreement with the observations of Fig. 4, where $\varepsilon_2 \ll \varepsilon_1$.

In Fig. 8, the relative error $|\varepsilon_{0,\mathrm{MC}} + \varepsilon_{1,\mathrm{MC}} - (\varepsilon_{0,\mathrm{EM}} + \varepsilon_{1,\mathrm{EM}})|/(\varepsilon_{0,\mathrm{MC}} + \varepsilon_{1,\mathrm{MC}})$ in percent is plotted versus the emission angle θ. The wind speeds $u_{12} = \{5, 10, 15, 20\}$ m/s and the wavelengths $\lambda = \{4, 10\}$ μm. For emission angles smaller than 80° and for wavelengths $\lambda = \{4, 10\}$ μm, the relative error does not exceed $\{0.4, 0.15\}$%, and does not exceed 0.9% for any emission angle and wavelength. Bourlier[6] showed that an accuracy in the sea surface temperature of 0.1 K (which corresponds approximately to the resolution of infrared cameras) implies accuracies in the relative error in emissivity of 0.42% for a wavelength of 4 μm, and of 0.17% for a wavelength of 10 μm. Hence for remote sensing applications ($\theta_1 < 80°$), the empirical model of ε_1 is accurate enough with this constraint. If the contribution of ε_1 is neglected, then the relative error is of the order of $\varepsilon_{1,\mathrm{MC}}/(\varepsilon_{0,\mathrm{MC}} + \varepsilon_{1,\mathrm{MC}}) \approx \varepsilon_{1,\mathrm{MC}} \in [0; 3.5]$%.

In Fig. 9, the parameters m_1 (top) and σ_1 (bottom) in degrees of the empirical function f [see Eq. (52)] are plotted versus the rms slope σ_s. The label "Fit" in the legend corresponds to the linear regression of $\{m_1 = a_{m_1} + b_{m_1}\theta, \sigma_1 = a_{\sigma_1} + b_{\sigma_1}\theta\}$. For wavelengths $\lambda = \{4, 10\}$ μm, $a_{m_1} = \{-114.9, -130.2\}$ degrees, $b_{m_1} = \{83.7, 87.2\}$, $a_{\sigma_1} = \{72.8, 81.1\}$ degrees, and b_{σ_1}

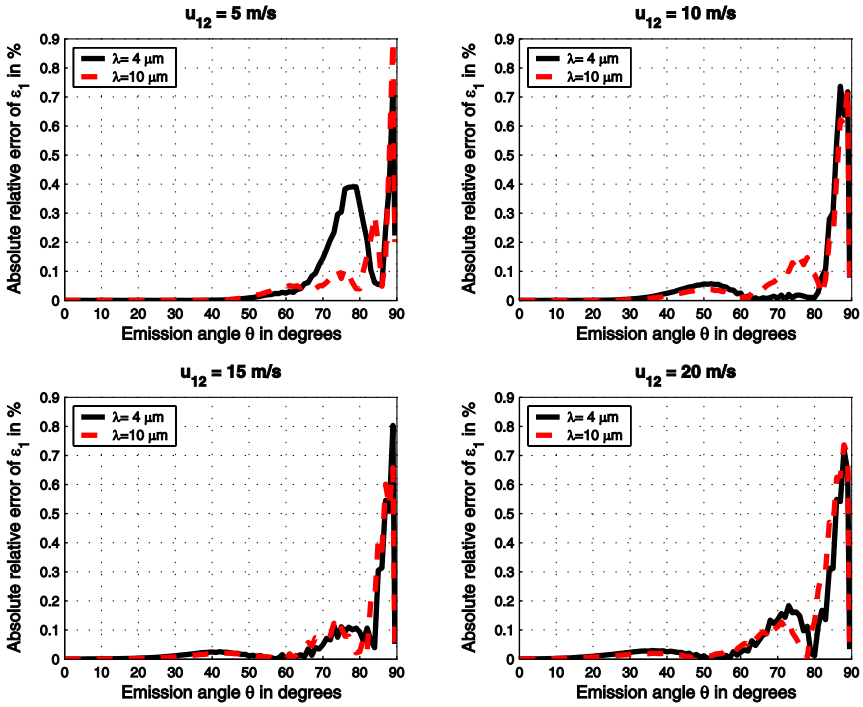

Fig. 8. (Color online) Absolute relative error $|\varepsilon_{0,\mathrm{MC}} + \varepsilon_{1,\mathrm{MC}} - (\varepsilon_{0,\mathrm{EM}} + \varepsilon_{1,\mathrm{EM}})|/(\varepsilon_{0,\mathrm{MC}} + \varepsilon_{1,\mathrm{MC}})$ in percent versus the emission angle θ. The wind speeds $u_{12} = \{5, 10, 15, 20\}$ m/s and the wavelengths $\lambda = \{4, 10\}$ μm.

$= \{11.1, 8.1\}$. One can observe that $\{m_1, \sigma_1\}$ weakly depend on the wavelength (the difference is $\pm 2°$), that m_2 decreases when the wind speed increases, which means that the maximum of ε_2 shifts towards lower emission angles; this is noticed in Fig. 7. On the other hand, as the wind speed increases, σ_1 increases, which means that the angular repartition of ε_1 is wider. This is consistent with Fig. 7. For A, one finds $A = 10.4$ for any wind speed and wavelength.

5. Conclusion

In this paper, from the geometric optics approximation, the unpolarized emissivity for a 2D stationary random rough surface is derived by taking the multiple reflections and the shadowing effect into account. The N-order statistical illumination function is derived and is included in the emissivity derivation. Closed-form expressions of the zero-, first- and second-order average illumination functions are given.

Numerical results of the zero-, first-, and second-order emissivities are presented by considering a 1D Gaussian sea surface, for wind speeds ranging from 5 to 20 m/s, for emission angles ranging from 0° to 90°, and for wavelengths equal to 4 and 10 μm. The simulations showed then that the contribution of the second-order emissivity is negligible in comparison to the zero- and first-order emissivities.

The analytical model is also compared with a Monte Carlo method. For the zero-order emissivity, a very good agreement between the analytical and the Monte Carlo methods is found, whereas for the second-order emissivity, the agreement between both models is poor. One then proved that this disagreement is due to the modeling of the first-order statistical illumination function, which underpredicts the illumination by a factor of 6. Nevertheless, the profiles of the emissivity and the average illumination function are similar for both models.

To obtain better agreement between the analytical and the Monte Carlo methods, an empirical model of the first-order emissivity is proposed. It consists in multiplying the analytical emissivity by a *simple* empirical function that depends on two parameters (the third is constant, $A = 10.4$). These parameters are obtained from the Monte Carlo approach. They depend linearly on the rms slope and weakly depend on the wavelength. A very good agreement is then found between the empirical and the Monte Carlo approaches, for which the relative error does not exceed

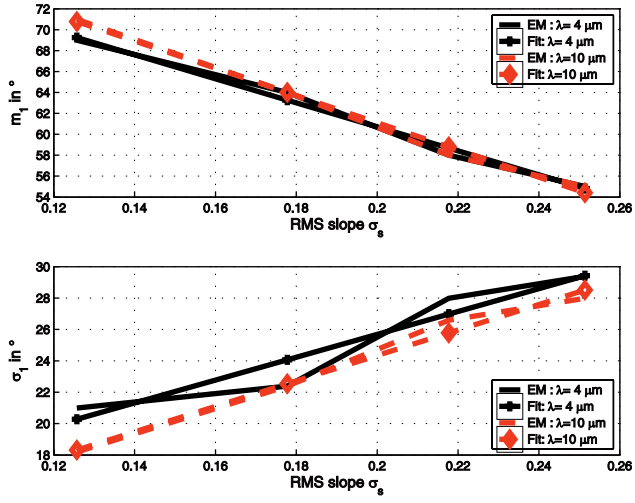

Fig. 9. (Color online) Parameters m_1 (top) and σ_1 (bottom) in degrees of the empirical function f versus the rms slope σ_s. The label "Fit" in the legend cor-responds to the linear regression of $\{m_1, \sigma_1\}$. The wavelengths $\lambda = \{4, 10\}$ μm.

0.4% for emission angles smaller than 80°, and 0.9% for any emission angle. For remote sensing applications, this is sufficient to have an accuracy of 0.1 K in the sea surface temperature.

The single reflection occurs for emission angles larger than 50° (this value decreases when the wind speed increases; see Fig. 7). This contribution is maximum for emission angles ranging from 60° to 80° and decreases above 80°. The first-order emissivity reaches a maximum of the order of 0.035, which weakly depends on the wind speed. From a Monte Carlo method, a good agreement is also observed between our emissivity model and the results of Henderson, Theiler, and Villeneuve,[11] in which they considered a 2D Gaussian anisotropic sea surface. This means that the contribution of the first-order unpolarized emissivity is similar for 1D and 2D sea surfaces.

From the analytical model, for a given emission angle, the computations of the zero-, first-, and second-order emissivities require a computing time of 0.7 μs, 44 μs, and 3.3 s, respectively. For the integrations over the surface slopes, the number of samples is $N_s = 80$, and one uses a personal computer (Pentium 4, CPU 3 GHz, 2 Gbytes of RAM) and Matlab software. For a 2D sea surface, for each order, the number of integrations is double, which implies that the computing time could be approximatively equal to $0.7 \times N_s$ μs = 56 μs and $44 \times N_s^2$ μs = 0.3 s for the zero- and first-order emissivities, respectively.

Appendix A: Expression of the First-Order Statistical Illumination Function of a Correlated Gaussian Process

In the downward direction ($z_0 \geq z_1$) and for a Gaussian correlated process of the surface heights and slopes at the points M_0 and M_1, the first-order statistical illumination function $S_1(\theta_1, \phi_1; M_1, M_0)$ is expressed as[12]

$$S_{0b}(\theta_1, \phi_1; M_1, M_0) = \begin{cases} \exp\left(-\int_0^{u_L} g\,du\right) & \text{if } 0 \leq \dfrac{h_0 - h_1}{\eta v_1} = u_L \leq u_t \\ \exp\left(-\int_0^{u_L} g\,du\right) G(v_1; h_1) & \text{otherwise} \end{cases}, \tag{A1}$$

in which

$$g(v_1; h_1, \zeta_1, h_0, u) = \frac{\eta}{\pi} \frac{\sqrt{f_{11}f_{33} - f_{13}^2}}{f_{33}} \times \frac{e^{-A-B-h_1^2-\zeta_1^2}\left[1 - \kappa\sqrt{\pi} e^{\kappa^2} \operatorname{erfc}(\kappa)\right]}{e^{B_1^2 - C_1}\left[1 + \operatorname{erf}\left(\sqrt{A_1} h_0 + B_1\right)\right]}. \tag{A2}$$

The functions $A(v_1; h_1, \zeta_1, h_0, u)$, $B(h_1, \zeta_1, h_0, u)$, $\kappa(v_1; h_1, \zeta_1, h_0, u)$, which appear in the numerator of g, are expressed as

$$A = \left[f_{33} v_1^2 + 2v_1(f_{34}\zeta_1 + f_{14}h_1 - f_{13}h_0)\right] f_M^{-1}, \tag{A3a}$$

$$B = \frac{f_{11}(h_1^2 + h_0^2) + 2f_{12}h_1h_0 + 2\zeta_1(f_{13}h_1 - f_{14}h_0) + f_{33}h_1^2}{f_M} - h_1^2 - \zeta_1^2, \tag{A3b}$$

$$\kappa = \frac{f_{14}h_1 - f_{13}h_0 + f_{34}\zeta_1 + f_{33}v_1}{\sqrt{f_{33}f_M}}. \tag{A3c}$$

The functions $A_1(u)$, $B_1(h_1, \zeta_1, u)$, $C_1(v_1; h_1, \zeta_1, u)$, which appear in the denominator of g, are expressed as

$$A_1 = (f_{11}f_{33} - f_{13}^2)/(f_{33}f_M) > 0, \tag{A4a}$$

$$B_1 = \frac{h_1(f_{12}f_{33} + f_{13}f_{14}) + \zeta_1(f_{13}f_{34} - f_{14}f_{33})}{\sqrt{f_{33}f_M(f_{11}f_{33} - f_{13}^2)}}, \tag{A4b}$$

$$C_1 = h_1^2 \frac{f_{11}f_{33} - f_{14}^2}{f_{33}f_M} + \zeta_1^2 \frac{f_{33}^2 - f_{34}^2}{f_{33}f_M} + 2h_1\zeta_1 \frac{f_{11}f_{33} - f_{14}f_{34}}{f_{33}f_M}. \tag{A4c}$$

In the above equations, the functions $\{f_{ij}(u)\}$, which depend only on u, are expressed as

$$\begin{aligned} f_{11} &= 1 - f_2^2 - f_1^2, \\ f_{33} &= 1 - f_0^2 - f_1^2, \\ f_{12} &= f_0 f_2^2 + f_2 f_1^2 - f_0, \\ f_{34} &= f_2 f_0^2 + f_0 f_1^2 - f_2, \\ f_{13} &= f_1(f_0 - f_2), \\ f_{14} &= f_1(1 - f_1^2 - f_0 f_2), \\ f_M &= (f_{33}^2 - f_{34}^2)/(1 - f_0^2), \end{aligned} \tag{A5}$$

in which $\{f_0(u), f_1(u), f_2(u)\}$ are given by

$$f_0 = C_0/\sigma_h^2, \quad f_1 = -C/(\sigma_h\sigma_s), \quad f_2 = -C_2/\sigma_s^2. \tag{A6}$$

σ_s and σ_h are the surface slope and height rms, respectively. $C_0(x)$ denotes the surface height correlation function and $\{C_{1,2}(x)\}$ its first and second derivatives with respect to $x = uL_c$. L_c is the surface height correlation length. In Eq. (A1), $\eta = \sigma_s L_c/\sigma_h$. For instance, for a Gaussian correlation function, one has $C_0(x) = \sigma_h^2 \exp(-x^2/L_c^2)$, which implies that

$$\begin{aligned}\sigma_s &= \sqrt{-C_2(0)} = \sqrt{2}\sigma_h/L_c,\\ \eta &= \sqrt{2},\\ f_0 &= \exp(-u^2),\\ f_1 &= u\sqrt{2}\exp(-u^2),\\ f_2 &= (1-2u^2)\exp(-u^2).\end{aligned} \tag{A7}$$

In fact, the use of the variable transformations

$$u = x/L_c, \quad h_{0,1} = z_{0,1}/(\sqrt{2}\sigma_h), \quad \zeta_0 = \gamma_0/(\sqrt{2}\sigma_s), \tag{A8}$$

allows the function g not to depend on $\{L_c, \sigma_h, \sigma_s\}$. In Eq. (A1), u_t corresponds to the lower value of u for which the correlation can be neglected, which occurs for $f_0(u) \to 0$. For a Gaussian correlation function, $u_t = 3$. Above this limit, $\{f_0, f_1, f_2\} \approx \{0, 0, 0\}$, which implies from Eq. (A5) that $f_{ij} = 1$ for $i = j$, 0 otherwise, and $f_M = 1$. The function g can then be simplified as

$$g = \frac{2\eta v_1 \Lambda_1 e^{-h_0^2}}{\sqrt{\pi}[1 + \mathrm{erf}(h_0)]} = g(v_1; h_0) \text{ for } u > u_t. \tag{A9}$$

In addition, $z_0 = z_1 + \mu_1(x_1 - x_0)$, in which $\mu_1 = |\cot \theta_1|$, and x_1 and x_0 are the abscissa of the points M_1 and M_0, respectively. With the variable transformations of Eq. (A8) and $x = x_1 - x_0 \geq 0$, this leads to $h_0 = h_1 + uv_1\eta$. For the case where $u > u_t$, the function G in Eq. (A1) is equal to $\exp[-s_{u_t}^{+\infty} g\mathrm{d}u]$. Thus the use of the above equation leads to

$$G(v_1; h_1) = \left[\frac{1 + \mathrm{erf}(h_1 + u_t v_1 \eta)}{2}\right]^{\Lambda_1} \text{ for } u > u_t. \tag{A10}$$

If one assumes that the above equation is valid for any u, for $u_t = 0$, $G(v_1; h_1) = \{[1 + \mathrm{erf}(h_1)]/2\}^{\Lambda_1}$ given by Eqs. (26) and (16) for an *uncorrelated* Gaussian process.

In the downward direction ($z_1 \geq z_0$), the first-order statistical illumination function is expressed from Eq. (A2) by substituting the variables $\{z_1, \zeta_1, z_0\}$ for $\{z_0, \zeta_0, z_1\}$.

For $M \Rightarrow z \to \infty \Rightarrow u \to \infty$, and $S(\theta_1, \phi_1; M_0, M)$ is then given by Eq. (A1), in which $u_L = u_t$. Moreover, in Eq. (A2), $h_1 = h_0 + uv_1\eta$.

The author thanks the reviewers for their relevant comments, which will influence the final appearance of this paper. The author also thanks N. Pinel for his comments.

References

1. X. Wü and L. Smith, "Emissivity of rough sea surface for 8–13 μm: modeling and verification," Appl. Opt. **36,** 2609–2619 (1997).
2. J. A. Shaw and C. Marston, "Polarized infrared emissivity for a rough water surface," Opt. Exp. **7,** 375–380 (2000).
3. P. D. Watts R. Allen, and T. J. Nightingale, "Wind speed effects on sea surface emission and reflection for the along track scanning radiometer," J. Atmos. Ocean. Technol. **13,** 126–141 (1996).
4. K. Masuda, T. Takashima, and Y. Takayama, "Emissivity of pure and sea waters for the model sea surface in the infrared window regions," Remote Sens. Environ. **24,** 313–329 (1988).
5. K. Yoshimori, K. Itoh, and Y. Ichioka, "Optical characteristics of a wind-roughened water surface: a two-dimensional theory," Appl. Opt. **34,** 6236–6247 (1995).
6. C. Bourlier, "Unpolarized infrared emissivity with shadow from anisotropic rough sea surfaces with non-Gaussian statistics," Appl. Opt. **44,** 4335–4349 (2005).
7. C. Bourlier, G. Berginc, and J. Saillard, "Theoretical study on two-dimensional Gaussian rough sea surface emission and reflection in the infrared frequencies with shadowing effect," IEEE Trans. Geosci. Remote Sens. **39,** 379–392 (2001).
8. C. R. Zeiss, C. P. MacGrath, K. M. Littfin, and H. G. Hughes, "Infrared radiance of the wind-ruffled sea," J. Opt. Soc. Am. A **16,** 1439–1452 (1999).
9. J. A. Shaw, "Polarimetric measurements of long-wave infrared spectral radiance from water," Appl. Opt. **38,** 379–392 (1999).
10. D. E. Freund, R. J. Joseph, D. J. Donohue, and K. T. Constantikes, "Numerical computations of rough sea surface emissivity using the interaction probability," J. Opt. Soc. Am. A **14,** 1836–1849 (1997).
11. B. G. Henderson, J. Theiler, and P. Villeneuve, "The polarized emissivity of a wind-roughened sea surface: a Monte Carlo model," Remote Sens. Environ. **88,** 453–457 (2003).
12. C. Bourlier, G. Berginc, and J. Saillard, "Monostatic and bistatic statistical shadowing functions from one-dimensional stationary randomly rough surface according to the observation length: part I. Single scattering," Waves Random Media **12,** 145–174 (2002).
13. C. Bourlier and G. Berginc, "Shadowing function with single reflection from anisotropic Gaussian rough surface. Application to Gaussian, Lorentzian, and sea correlations," Waves Random Media **13,** 27–58 (2003).
14. C. Bourlier, G. Berginc, and J. Saillard, "Monostatic and bistatic statistical shadowing functions from one-dimensional stationary randomly rough surface according to the observation length: part II. Multiple scattering," Waves Random Media **12,** 175–200 (2002).
15. A. G. Pavel'yev, *Double Scattering by a Random Irregular Surface* (Scripta Publishing, 1984), pp. 5–15.
16. G. M. Hale and M. R. Querry, "Optical constants of water in the 200-nm to 200-mm wavelength region," Appl. Opt. **12,** 555–563 (1973).
17. C. Cox and W. Munk, "Measurement of the roughness of the sea surface from photographs of the suns glitter," J. Opt. Soc. Am. **44,** 838–850 (1954).